

N_3^+ : Full-Dimensional Potential Energy Surface, Vibrational Energy Levels and Ground State Dynamics

Debasish Koner,[†] Max Schwilk,[†] Sarbani Patra,[†] Evan J. Bieske,[‡] and Markus
Meuwly^{*,¶}

[†]*Department of Chemistry, University of Basel, Klingelbergstrasse 80, CH-4056 Basel,
Switzerland*

[‡]*Department of Chemistry, University of Melbourne, Parkville 3010, Australia*

[¶]*Department of Chemistry, University of Basel,
Klingelbergstrasse 80, 4056 Basel, Switzerland*

E-mail: m.meuwly@unibas.ch

April 28, 2020

Abstract

The fundamentals and higher vibrationally excited states for the N_3^+ ion in its electronic ground state have been determined from quantum bound state calculations on 3-dimensional potential energy surfaces (PESs) at the CCSD(T)-F12 and MRCI+Q levels of theory. The vibrational fundamentals are at 1130 cm^{-1} (ν_1 , symmetric stretch), 807 cm^{-1} (ν_3 , asymmetric stretch), and 406 cm^{-1} (ν_2 , bend) on the higher-quality CCSD(T)-F12 surface. For ν_1 , the calculations are close to the estimated frequency from experiment (1170 cm^{-1}) and previous calculations [Chambaud *et al.*, Chem. Phys. Lett., 1994, 231, 9–12] which find it at 1190 cm^{-1} . Calculations of the vibrational states

on the MRCI+Q PES are in qualitative agreement with those using the CCSD(T)-F12 PES. Analysis of the reference CASSCF wave function for the MRCI+Q calculations provides further insight into the shape of the PES and lends support for the reliability of Hartree-Fock as the reference wave function for the coupled cluster calculations. According to this, N_3^+ has mainly single reference character in all low-energy regions of its electronic ground state ($^3A''$) 3d PES.

Introduction

N_3^+ is an ion involved in the chemistry of atmospheres, plasmas and discharges. It has been found, alongside with O_3^+ , to play an important role in electrical discharges in air.¹ Together with N_4^+ , N_3^+ has been suggested to be the most abundant nitrogen ion in the lower atmosphere of Titan where it is formed through ternary reactions between N^+ and $N_2(\Sigma_g^+)$.² As a consequence of its importance, Fourier transform mass spectrometric studies of N_3^+ reacting with several oxides were carried out in order to characterize the resulting products.¹ The reactions are of particular relevance when urban pollutants or greenhouse gases, such as SO_2 , N_2O , or CO_2 are involved, where typical reactions include $N_3^+ + SO_2 \rightarrow NO^+ + SO + N_2$ and $N_3^+ + N_2O \rightarrow NO^+ + 2N_2$. In these reactions, N_3^+ is an N^+ donor participating in the general reaction scheme $N_3^+ + XYZ \rightarrow NXYZ^+ + N_2$ with subsequent decomposition of $NXYZ^+$. Another process relevant in Earth's atmosphere is the charge transfer reaction $N(^4S) + N_2^+(X^2\Sigma_g^+) \rightleftharpoons N^+(^3P) + N_2(X^1\Sigma_g^+)$ where N_3^+ is believed to be formed through the association reaction $N^+ + N_2 \rightarrow N_3^+$.³ Finally, N_3^+ has also been implicated in the NO^+ production reaction $N_3^+ + NO \rightarrow NO^+ + N_2 + N$.⁴

Experimentally, rotationally resolved $A^3\Pi_u \leftarrow X^3\Sigma_g^-$ electronic spectra of N_3^+ have been recorded by monitoring N^+ photo-products as a function of excitation wavelength (over the 245 to 283 nm range).⁵ Analysis of the ro-vibronic transitions established that in its ground electronic state N_3^+ possesses a linear, centrosymmetric ($D_{\infty h}$) structure, with an

N-N bond length of 1.193 Å. Although the vibrational frequencies for the X $^3\Sigma_g^-$ state could not be measured directly, it was expected that they are lower than those of the A $^3\Pi_u$ state, which were $\nu_1 \approx 1300 \text{ cm}^{-1}$, $\nu_2 \approx 440 \text{ cm}^{-1}$, and $\nu_3 \approx 1700 \text{ cm}^{-1}$, respectively.⁵ This is also consistent with a value of $\nu_1 = 1170 \text{ cm}^{-1}$ for the ground state of N $_3^+$, which was deduced from photoelectron spectroscopy.⁶

The first comprehensive computational study of N $_3^+$ used a complete active space self-consistent field (CASSCF) approach and multireference configuration interaction singles and doubles method (MRCI) to calculate vertical excitation energies and specify the collinear dissociation paths of the electronically excited states.³ Earlier attempts to theoretically investigate the structure of the N $_3^+$ ion were inconclusive, with studies identifying a linear N $_3^+$ molecule with either $C_{\infty v}$ geometry^{7,8} or $D_{\infty h}$ ⁹ symmetry for the ground state. Using highly correlated Complete Active Space SCF followed by multireference Averaged Coupled Pair Functional (CASSCF-ACPF) calculations it was possible to establish the ground state $D_{\infty h}$ structure.¹⁰ An exploratory calculation at the MP2/aug-cc-pVTZ level of theory found that the correct symmetric geometry with N-N bond lengths of 1.164 Å is only obtained if the initial structure is close to the ground state geometry. Conversely, starting with a linear asymmetric structure, the ground state geometry converged to one with $C_{\infty v}$ symmetry with N-N bond lengths $r_{\text{N1-N2}} = 1.441 \text{ Å}$ and $r_{\text{N2-N3}} = 1.069 \text{ Å}$. This finding is also consistent with that obtained earlier at the MRCI level of theory with a double zeta plus polarization (DZ+P) basis set⁸ for which the respective calculated bond lengths were $r_{\text{N1-N2}} = 1.43 \text{ Å}$ and $r_{\text{N2-N3}} = 1.20 \text{ Å}$.

Vibrational calculations on a potential energy surface (PES) calculated at the CASSCF level of theory found the vibrational fundamentals at $\nu_1 = 1190 \text{ cm}^{-1}$, $\nu_2 = 426 \text{ cm}^{-1}$, and $\nu_3 = 929 \text{ cm}^{-1}$.¹⁰ Subsequent *ab initio* MD simulations (10 ps) at the B3PW91/6-31G** level of theory predicted the fundamentals at $\nu_1 = 1040 \text{ cm}^{-1}$, $\nu_2 = 393 \text{ cm}^{-1}$, and $\nu_3 = 900$

cm^{-1} from analyzing the Fourier transform of the velocity autocorrelation function.¹¹ These frequencies also display the (unusual) situation that the antisymmetric stretch vibration lies lower in frequency than the symmetric stretch. Notably, the wavenumber of the symmetric stretch is 130 cm^{-1} below the experimental value,⁶ and also considerably below that determined from the earlier bound state calculations.¹⁰

Here, in order to provide a more definitive characterization of the potential energy surface for N_3^+ and the vibrational states supported by it, high-level electronic structure calculations are combined with state-of-the-art methods to represent 3-dimensional PESs and quantum bound state calculations. This work is also a prerequisite for investigating the photodissociation dynamics for the excited states of N_3^+ .

Computational Methods

First the generation and representation of the 3-dimensional PES for N_3^+ is described. This PES is then used for computing the vibrational bound states using methods to solve the time-dependent and time-independent nuclear Schrödinger equation.

The Ground State PES for N_3^+

All electronic structure calculations were performed using the Molpro 2019.1^{12,13} software. The PES for N_3^+ has been determined at two different levels of theory. First, calculations at the CCSD(T)-F12b¹⁴/aug-cc-pVTZ-f12¹⁵ level with the corresponding density fitting and a resolution of the identity basis sets in the F12 computation provide a high quality ground state PES. A spin-restricted open-shell Hartree-Fock reference wave function was used for the spin unrestricted coupled cluster wave function. Secondly, MRCI^{16,17}/aug-cc-pVTZ¹⁸ with the Davidson quadruples correction¹⁹ (MRCI+Q) calculations with a CASSCF²⁰⁻²³ refer-

ence wave function were carried out in view of future explorations of the photo-dissociation process which require fully-dimensional PESs for electronically excited states.

For CASSCF the active space was the full valence space and the calculations were performed as state-averaged calculations including the two lowest singlet and triplet spin states of A' and A'' symmetry, respectively. Multi-reference effects are potentially important in certain regions of the PES. For this, an analysis of the CASSCF wave function provides additional information about the reliability of the Hartree-Fock reference wave function for the coupled cluster calculations. Furthermore, for the dissociation $N_3^+ \rightarrow N_2 + N^+$ the role of the energetically adjacent $N_2^+ + N$ state can also be discussed based on analyzing the CASSCF wave function.

Jacobi coordinates (R, r, θ) were used to define the molecular geometry. Here, r is the separation between nitrogen N1 and N2, R is the distance between N3 and the center of mass of N1 and N2, and θ is the angle between \vec{r} and \vec{R} , see Figure 1. The angular grid is defined by Gauss-Legendre quadrature points between 0 and 90° considering the symmetry of the system. Details of the angular and radial grids for the CCSD(T)-F12b and MRCI+Q calculations are given in Table ??.

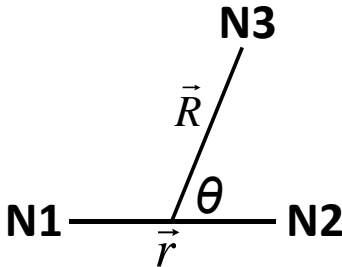


Figure 1: The coordinate system (R, r, θ) used for the 3-dimensional PES for N_3^+ . The vector \vec{r} is the N1–N2 separation, \vec{R} is the separation between N3 and the center of mass of N1–N2, and θ is the angle between the two distance vectors.

In addition, the PES of N_2 is required in order to correctly describe the long-range asymptotic

behaviour. Calculations of the N_2 energies were carried out at the same level of theory as for the underlying 3-dimensional PESs. The 1-dimensional curve for N_2 was then represented by a 1-dimensional reproducing kernel Hilbert space (RKHS, see below). With this, the energy of N_3^+ is

$$V(R, r, \theta) = E(R, r, \theta) + E_{N_2}(r) \quad (1)$$

where $E(R, r, \theta)$ is the interaction energy of the $N^+ + N_2$ system and $E_{N_2}(r)$ is the energy of the N_2 molecule (N1-N2).

Reproducing Kernel Representation of the 3d-PES for N_3^+

To represent the 3- and 1-dimensional energies $E(R, r, \theta)$ and $E_{N_2}(r)$ a reproducing kernel Hilbert space (RKHS) interpolation scheme is used.^{24,25} Starting from N known values $f(\mathbf{x}_i)$ for coordinates \mathbf{x}_i , the RKHS theorem states that for arbitrary values \mathbf{x} the function $f(\mathbf{x})$ can be evaluated as a linear combinations of kernel products

$$f(\mathbf{x}) = \sum_{i=1}^N \alpha_i K(\mathbf{x}, \mathbf{x}_i), \quad (2)$$

where α_i are the coefficients and $K(\mathbf{x}, \mathbf{x}_i)$ are the reproducing kernels. The coefficients can be evaluated from the known values $f(\mathbf{x}_i)$ by solving a set of linear equations

$$f(\mathbf{x}_j) = \sum_{i=1}^N \alpha_i K(\mathbf{x}_i, \mathbf{x}_j). \quad (3)$$

Thus, a RKHS exactly reproduces the input data at the reference points \mathbf{x}_i . However, for noisy data a small damping value is added to the diagonal elements to regularize the data set. The derivatives of $f(\mathbf{x})$ can be calculated analytically from the kernel functions $K(\mathbf{x}, \mathbf{x}')$. For a multidimensional function the D -dimensional kernel can be constructed as the product

of D 1-dimensional kernels $k(x, x')$

$$K(\mathbf{x}, \mathbf{x}') = \prod_{d=1}^D k^{(d)}(x^{(d)}, x'^{(d)}), \quad (4)$$

where $k^{(d)}(x^{(d)}, x'^{(d)})$ are the 1-dimensional kernels for the d -th dimension.

In the present work, the explicit form of the reciprocal power decay kernel polynomials are used for the radial coordinates. Kernel functions ($k^{[n,m]}$) with smoothness $n = 2$ and asymptotic decay $m = 4$ are used for the R dimension

$$k^{[2,4]}(x, x') = \frac{2}{15} \frac{1}{x_{>}^5} - \frac{2}{21} \frac{x_{<}}{x_{>}^6}, \quad (5)$$

while $n = 2$ and $m = 6$ is used for the r dimension

$$k^{[2,6]}(x, x') = \frac{1}{14} \frac{1}{x_{>}^7} - \frac{1}{18} \frac{x_{<}}{x_{>}^8}, \quad (6)$$

where, $x_{>}$ and $x_{<}$ are the larger and smaller values of x and x' , respectively. Such a kernel smoothly decays to zero maintaining the correct leading term in the asymptotic region, and giving the correct long-range behavior for atom-diatom type interactions. For the angular dimension θ a Taylor spline kernel is used:

$$k^{[2]}(z, z') = 1 + z_{<}z_{>} + 2z_{<}^2z_{>} - \frac{2}{3}z_{<}^3, \quad (7)$$

Here, $z_{>}$ and $z_{<}$ are the larger and smaller values of z and z' , respectively, and z is defined as

$$z = \frac{1 - \cos\theta}{2}, \quad (8)$$

so that the values of $z \in [0, 1]$.

Finally, the 3-dimensional kernel is

$$K(\mathbf{x}, \mathbf{x}') = k^{[2,4]}(R, R')k^{[2,6]}(r, r')k^{[2]}(z, z'), \quad (9)$$

where, \mathbf{x}, \mathbf{x}' are (R, r, z) and (R', r', z') , respectively. The coefficients α_i and the RKHS representation of the PES are evaluated by using a computationally efficient toolkit.²⁵

Bound State Calculations

The bound states supported by the PESs considered in the present work were calculated using the DVR3D suite of codes.²⁶ The nuclear time-independent Schrödinger equation for N_3^+ is solved in a discrete variable representation (DVR) grid in Jacobi coordinates. The angular degree of freedom is defined by 56 Gauss-Legendre quadrature points while the radial degrees of freedom are defined by Gauss-Laguerre quadratures, 72 points along R and 48 points along r . The angular basis functions are expressed as Legendre polynomials while the radial basis functions are constructed using Morse oscillator functions with $r_e = 2.25 a_0$, $D_e = 0.32E_h$ and $\omega_e = 0.008E_h$ for r , and with $R_e = 3.8 a_0$, $D_e = 0.15E_h$ and $\omega_e = 0.0015E_h$ for R . With these parameters the r grid extends from 1.38 to 3.07 a_0 while the R grid covers the range between 1.60 and 5.91 a_0 . The r_2 embedding is used to calculate the rotationally excited states, where the z -axis is parallel to R in body-fixed Jacobi coordinates. The vibrational wave functions are transformed from Jacobi coordinates to symmetric $(R_{\text{N}_1\text{N}_2} + R_{\text{N}_2\text{N}_3})/\sqrt{2}$, asymmetric $(R_{\text{N}_1\text{N}_2} - R_{\text{N}_2\text{N}_3})/\sqrt{2}$ and bending coordinates using a Gaussian kernel-based interpolation method where the terminal N atoms are N1 and N3 while the middle N atom is N2. The bending coordinate is $\angle \text{N}_1\text{N}_2\text{N}_3$. Quantum numbers associated with the vibrational wave functions are assigned by counting the nodal planes along each coordinate.

As an independent validation of the vibrational frequencies, time dependent quantum me-

chanical (TDQM) calculations were carried out to determine the bound states for $J = 0$. In this approach an autocorrelation function is computed from the time propagation of an initial wave packet followed by Fourier transformation to compute the energy spectrum.²⁷⁻²⁹ The initial wave packet is a product of two Gaussian functions along the radial (R, r) coordinates and a function based on normalized associated Legendre polynomials describes the angular coordinates. The initial wavepacket (WP) is located at $R = 3.6 a_0$ and $r = 2.1 a_0$. The R grid consists of 108 evenly spaced points from 1.55 to 9.575 a_0 while the r grid has 70 points with a span from 1.1 to 4.55 a_0 . The angular grid was defined by 56 Gauss-Legendre quadrature points. The split operator method is used to compute the time evolution of the WP.³⁰ A sine damping function is multiplied to the WP near the grid boundary to avoid unphysical reflections from it. The autocorrelation function $A(t) = \langle \psi_0 | \psi_t \rangle$ is calculated at each time step. Finally the eigen energy spectrum was obtained from the Fourier transform of $A(t)$. A window function (Normalized Hanning or Gaussian) is used to reduce the noise in the spectra.^{31,32} The peak positions are then determined by fitting a Gaussian function to each peak.

Results and Discussion

The Ground State Potential Energy Surface

Ab initio energies up to 10 eV from the N_3^+ atomization energy ($E_N + E_N + E_{N^+}$) computed at the CCSD(T)-F12b and MRCI+Q levels of theory are used as input for the RKHS to construct the PESs. First, the quality of the RKHS representation was assessed. Figure SI1 compares the *ab initio* energies at the two different levels of theory with those obtained from RKHS interpolations. The correlation coefficients (R^2) between the reference calculations (CCSD(T)-F12b and MRCI+Q) and the RKHS representation are $1 - 4 \times 10^{-7}$ and $1 - 3 \times 10^{-7}$, respectively, for energies up to 6 eV, see Figure ??

Furthermore, energies for 219 and 252 off-grid points were computed at the CCSD(T)-F12b and MRCI+Q levels of theory, respectively, and the corresponding energies from the 3d-RKHS PESs were evaluated. For the CCSD(T)-F12b/aug-cc-pVTZ-f12 and MRCI+Q/aug-cc-pVTZ PESs the respective correlation coefficients are 0.9999 and 0.9993 (Figure ??). Selected 1D cuts along R for different values of r and θ are shown in Figure 2. These comparisons establish the high quality of the representation of the PES.

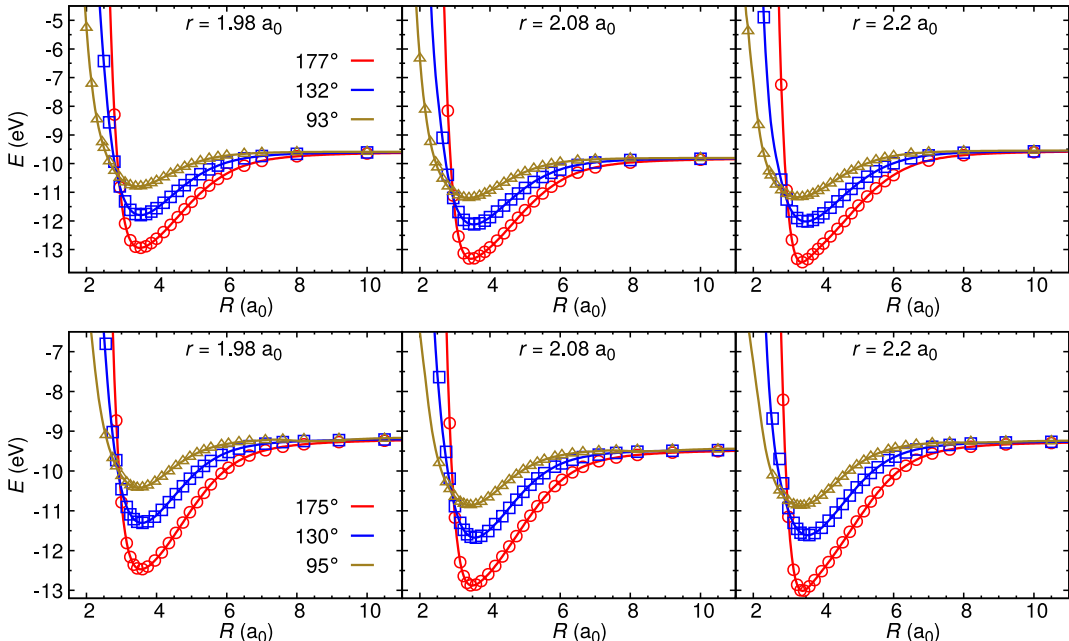


Figure 2: Comparison between the *ab initio* and RKHS interpolated energies as a function of R . Upper panel represents the CCSD(T)-F12b PES and lower panel represents the MRCI+Q PES.

A 2-d projection for an N1-N2 separation of $2.080 a_0$ is shown in Figure 3 for both PESs. The linear configurations show a deep minimum, which is the global minimum for the system. For the CCSD(T)-F12b PES, the global minimum lies 3.649 eV below the $\text{N}^+ + \text{N}_2$ asymptote for $r_{\text{NN}} = 2.243 a_0$. This compares well with the minimum obtained from electronic structure calculations as $2.244 a_0$. For the MRCI+Q PES the global minimum is 3.591 eV below the $\text{N}^+ + \text{N}_2$ asymptote for a linear symmetric structure with $r_{\text{NN}} = 2.256 a_0$. Two-dimensional

cuts in internal coordinates are provided in Figure 4 for the equilibrium region which shows the symmetric nature of the PES.

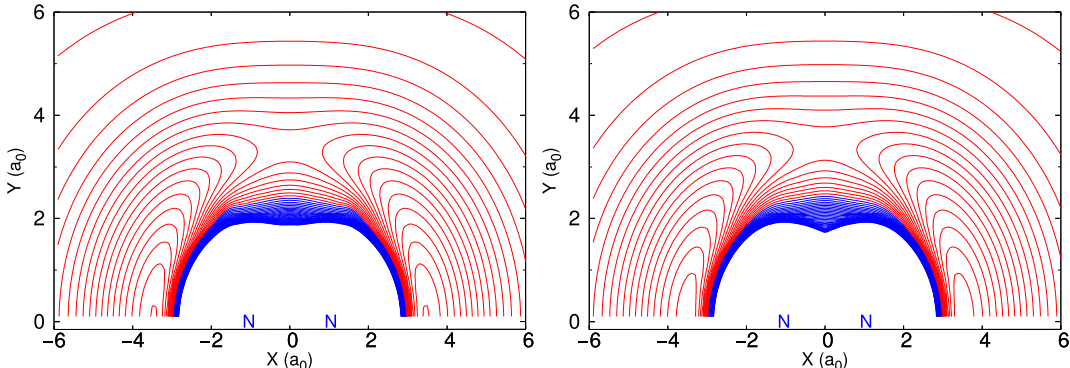


Figure 3: Contour diagram for the analytical PESs (left: CCSD(T)-F12b PES and right: MRCI+Q PES) for $r = 2.080 a_0$. Contour spacings are 0.2 eV. Blue and red lines represent positive and negative energies, respectively. The zero of energy is at the $N^+(^3P) + N_2(X^1\Sigma_g^+)$ asymptote.

Electronic Structure of the Ground State PES

Molecular orbital (MO) diagrams for the bonding of N^+ to N_2 shown in Figure 5 (“end-on”) and Figure 6 (“side-on”) help explain the topography of the PES in Figure 3. The MOs are obtained as CASSCF natural orbitals of the valence space (i. e. the active space) and their occupation is determined from the one or few dominant CASSCF CI vectors. Ground state ($X^3\Sigma_g^-$) linear N_3^+ has two degenerate, singly occupied non-bonding π_3 orbitals. Since the singly occupied orbitals of the triatomic complex smoothly transform into degenerate p -orbitals on $N^+(^3P)$ upon linear dissociation, a triplet ground state with one dominant configuration contributing to the CASSCF wave function (normalized square norm of the CI coefficient $> 65\%$) persists along the entire path. This characteristic also explains the absence of a repulsive region at long range as a consequence of an avoided crossing (see Figure 2 at $\theta = 175^\circ$). A more detailed evolution of the corresponding CASSCF natural orbitals is shown in Figure ???. For covalent bonding distances $r \approx R$ the natural orbitals

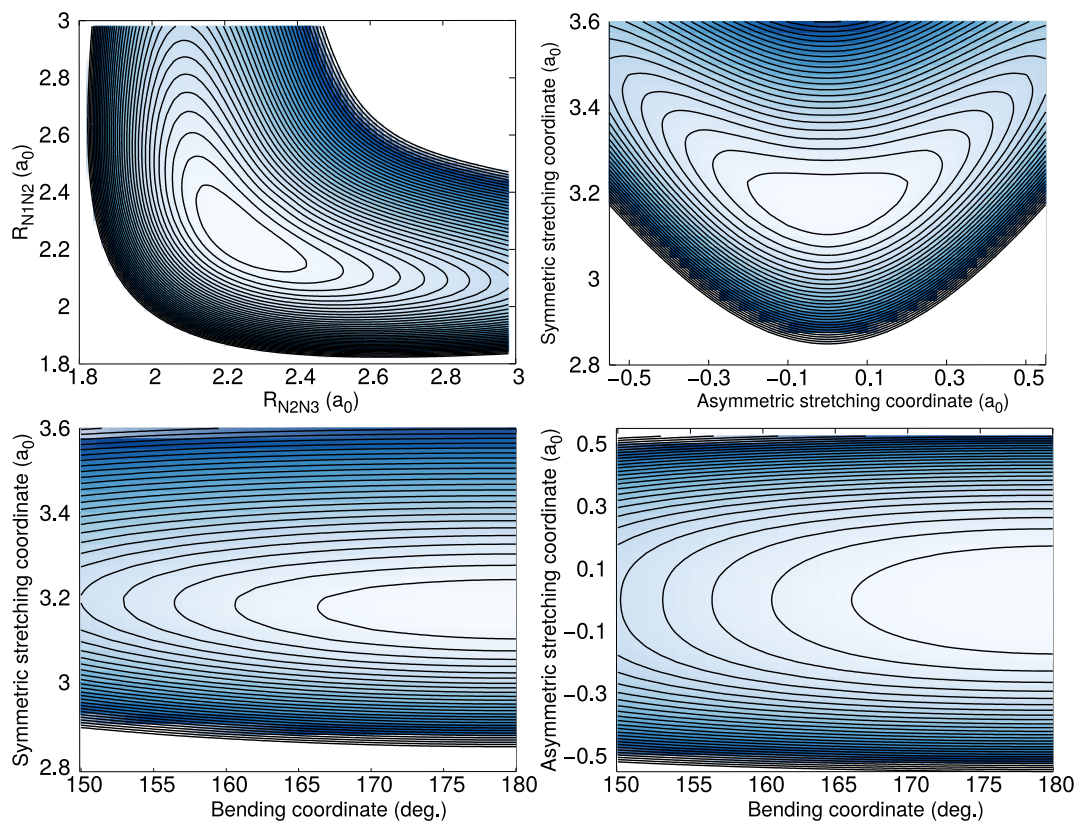


Figure 4: Contour and color map representation of the the CCSD(T)-F12b RKHS PES. Upper left: In internal coordinates, R_{N1N2} vs. R_{N2N3} with fixed $\angle(N1N2N3) = 180^\circ$. Upper right: In symmetric, asymmetric stretching, coordinates with fixed $\angle(N1N2N3) = 180^\circ$. Lower left: In symmetric stretching and bending coordinates with a value of zero for the asymmetric stretching. Lower right: In asymmetric stretching and bending coordinates with a fixed value of $3.1725 a_0$ for the symmetric stretching coordinate. Spacing between the contours is 500 cm^{-1}

are symmetry-adapted 3-center bonds and their energy ordering is essentially determined by their π - or σ - character and the number of nodal planes that partition the bond axis.

A triplet state “side-on” bonding of N^+ to N_2 also occurs along a dissociation path without an avoided crossing of two electronic states (with the absence of repulsive barrier in the 1-D dissociation curve in Figure 2 at $\theta = 95^\circ, 130^\circ$) and one dominant triplet state electron configuration. An MO diagram of the valence space CASSCF natural orbitals is shown in Figure 6 with more details reported in Figure ???. The degeneracy of the singly occupied orbitals breaks upon bending of the linear structure. The two singly occupied orbitals in the triplet state remain quasi-degenerate upon slight to moderate bending of the linear molecule. Only for structures close to an equilateral triangle the lowest singlet and triplet states are energetically close. The singlet state is lower in energy than the triplet state only in a small region of the PES, namely for $r \lesssim 2.3 a_0$, $R \lesssim 2.6 a_0$ and $\theta \approx 90^\circ$. This triangular structure with approximately equidistant atoms is, however, more than ≈ 2.8 eV above the absolute minimum of the PES (see Figure 3) at the MRCI+Q level of theory. Hence, it can be assumed that the excited singlet state’s role on the molecular dynamics of the ground state is minor.

Remarkably, the transition from the linear to the triangular structure on the triplet state evolves along one dominant CASSCF configuration. This occurs because of a smooth transformation along the reaction channel of the singly occupied π_3 non-bonding orbitals in the linear structure to the singly occupied orbitals in the T-shaped structure. Comparing these orbitals in Figures 5 and 6 indicate that the planes of antisymmetry are conserved. Such a one-to-one mapping emerges for all orbitals in the linear and T-shaped structure and energy reordering of them along the reaction channel only occurs in ways that do not qualitatively change the occupation number of a natural orbital.

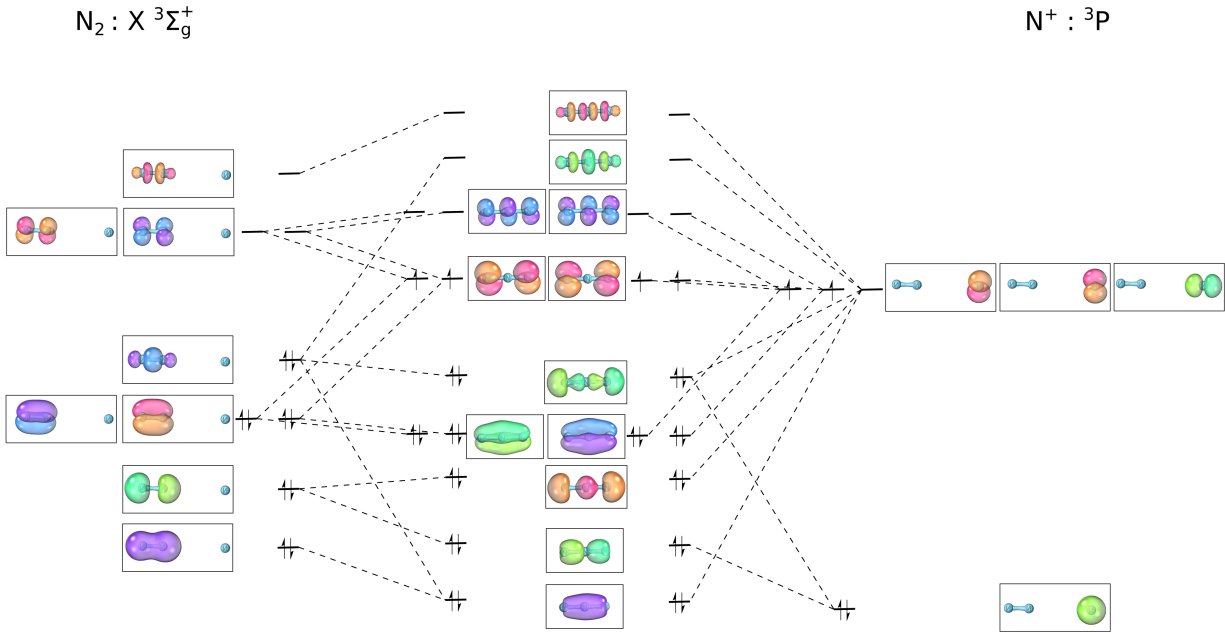


Figure 5: MO diagram of the CASSCF valence space natural orbitals for linear bonding of N^+ to N_2 . Single occupation of the degenerate π_3 -nonbonding orbitals leads to a triplet ground state. Orbital visualization has been performed with IboView.³³ The orbital isosurfaces enclose 80% of the electron density.

It should be noted that the degeneracy of the three occupation configurations of the p -orbitals in the 3P state of N^+ can be interpreted as a multireference character of N^+ . However, the coupling of the three states in the Hamiltonian can always be removed by appropriate orbital rotations even for the N^+-N_2 Van der Waals complex. Therefore, a meaningful Hartree-Fock solution also exists in these cases. In this context, it should be noted that the difference in energy stemming from the difference in Hartree-Fock and CASSCF occupied orbitals is strongly reduced by the subsequent coupled cluster or MRCI computations, as the singles excitations in the correlated methods effectively act as correcting orbital rotations under the (higher-order) electron correlation effects.

In summary, for an only mildly stretched N1-N2 covalent bond ($r < 2.7 a_0$), changes of R and θ can be qualitatively correctly described by a smooth evolution of a wave function with one dominant triplet configuration. This explains why open-shell unrestricted coupled clus-

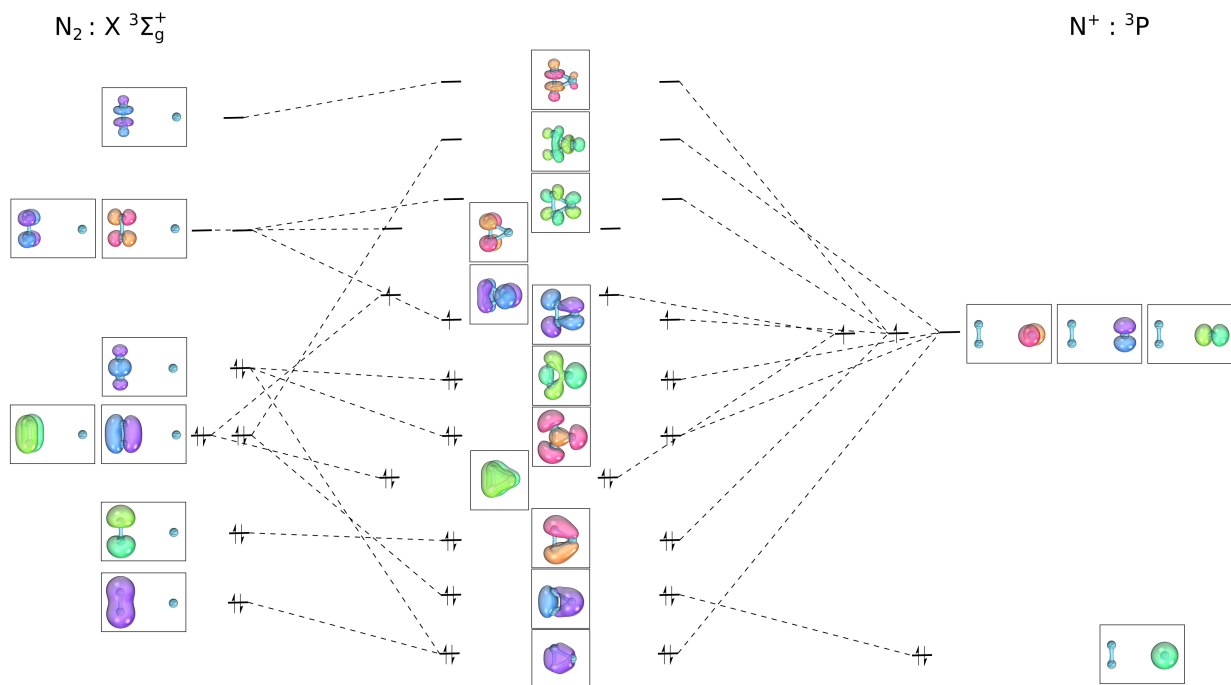


Figure 6: MO diagram of the valence space natural orbitals for the T-shaped bonding of N^+ to N_2 . The nitrogen p -orbitals recombine to form frontier MOs with different nodal structures that are close in energy but not degenerate.

ter with a triplet state restricted Hartree-Fock reference wave function performs very well in this region of the PES. It is also interesting to note that the ground state electronic structure of N_3^+ bears characteristics similar to those of molecular oxygen, a very stable triplet ground state molecule.

When the values of r and R both increase towards dissociation, the multireference character of the systems quickly becomes significant. Here only a full valence space CASSCF wave function can be a reliable reference wave function. In the dissociation region two energetically closely lying states emerge which are related by charge transfer. Experimentally, N^+N_2 is energetically favoured over $\text{N}+\text{N}_2^+$ by 1.05 eV which is the difference in the first ionization energies of N_2 (15.58 eV; Ref.³⁴) and that of atomic nitrogen (14.53 eV; Ref.³⁵). At the CASSCF and MRCI+Q levels of theory, the computed ionization energies of N_2 are 16.33 eV and 15.52 eV, respectively, whereas those of atomic nitrogen are 13.37 eV and 14.45 eV. Thus, MRCI+Q yields ionization energies in good agreement with experiment whereas CASSCF does not.

For stretched N_2 with $r = 3.0 a_0$ the charge transfer reaction energy of $\text{N}^+\text{N}_2 \rightarrow \text{N}+\text{N}_2^+$ is 0.84 eV and -0.38 eV at the CASSCF and MRCI+Q level of theory, respectively. Therefore, the triplet ground state may become the charge transfer state associated with the $\text{N}+\text{N}_2^+$ dissociation limit. Even though these are rather high-energy regions of the PES, this aspect has to be monitored, as the CASSCF algorithm will converge to different solutions depending on the initial orbital guess if the natural orbitals between which the charge transfer occurs are spatially sufficiently separated and can therefore not mix. Figure 7 illustrates such a case: at $r = 3 a_0$ two different CASSCF solutions for the lowest $^3\text{A}''$ state are obtained depending on the initial orbital guess for values of R above $\approx 6 a_0$. The natural orbital pairs of the charge transfer are shown as inset and their slight difference in spatial extent stems of the neutral or cationic character of the moieties.

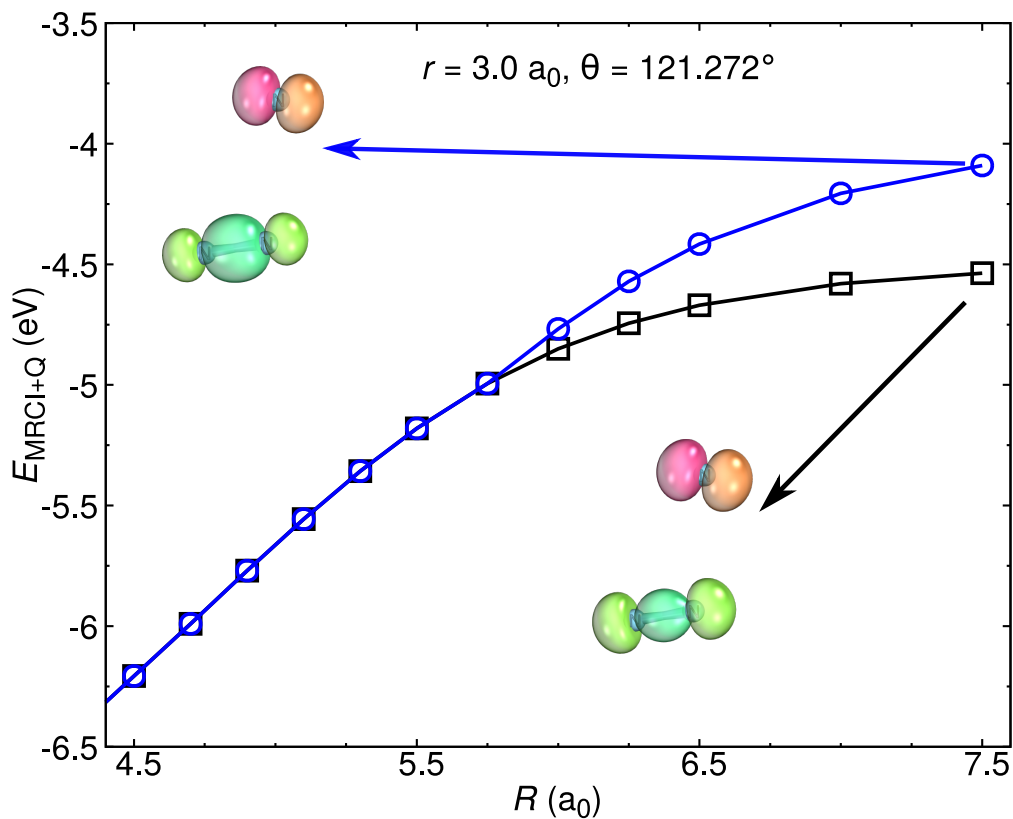


Figure 7: 1D cut of the *ab initio* PES along R for $\theta = 121.272^\circ$ and $r = 3.0 a_0$. Branching of the CASSCF solution that occurs when using initial guesses of orbitals that are connected to the $\text{N}^+ + \text{N}_2$ (blue) and $\text{N} + \text{N}_2^+$ (black) dissociation. Note the slight difference in spatial extent of the CASSCF natural orbitals (respective HOMOs of the two monomers, the density isosurface encloses 80% of the electron density).

In the region strong orbital mixing (formation of the covalent bond) the two charge transfer states ($N^+ + N_2$ and $N + N_2^+$) must mix and therefore have to go through a conical intersection. The N_3^+ excited states that connect to this conical intersection for values of R smaller than the covalent bond limit ($R \lesssim 5.5 a_0$), involve occupation of one of the antibonding orbitals of N_3^+ and therefore steeply increase in energy for decreasing values of R .³ In fact, the MO diagrams in Figures 5 and 6 indicate that the singly occupied orbitals of the N_3^+ ground state involve the p_x and p_y orbitals of N^+ . The orbital connections for collinear $N^+ + N_2$ in the MO diagram of Figure 5 only exist for orbitals with the same irreducible representation in $C_{\infty v}$, the point group that is preserved along the collinear reaction channel. An electron count then yields that the π -system of the N_3^+ ground state can only be connected to the 3P N^+ state with occupied p_x and p_y orbitals, as indicated. The two other of the three degenerate 3P states of N^+ then necessarily connect to a high lying excited state of N_3^+ with an occupied σ^* orbital. This is also consistent with earlier results.³

In summary, for values of R smaller than in the immediate region of the covalent bond formation between the N_2 and N moieties all (near-)degeneracies of the different triplet states are lifted and restricted open shell Hartree-Fock is a meaningful reference wave function.

Vibrational Spectrum

The vibrational levels of the N_3^+ ion were obtained by solving the nuclear Schrödinger equation using the DVR3D²⁶ suite of programs. The absolute and relative energies for the $J = 0$ states on the CCSD(T)-F12 and MRCI+Q PESs using DVR3D and the solution of the time dependent nuclear Schrödinger equation are given in Table 1. A few representative wavefunctions for the lower levels are reported in Figure 8 and additional ones are given in Figures ?? to ??.

The results in Table 1 demonstrate that solutions from the time-independent and time-dependent nuclear Schrödinger equation are very close to one another - typically within less than 1 cm^{-1} . Hence, these energies can be considered converged. On the other hand the absolute energies between the two PESs can differ by up to 90 cm^{-1} . Given that a single reference treatment of the electronic structure for the deeply bound region is a good approximation it is expected that the results on the CCSD(T)-F12 PES are more accurate than those on the MRCI+Q PES.

Table 1: The 20 lowest bound states (in cm^{-1}) for N_3^+ with $J = 0$ obtained from DVR3D and TDQM calculations on the CCSD(T)-F12b and MRCI+Q PESs. The zero of energy is set at the minimum of the PES.

CCSD(T)-F12b					MRCI+Q				
n	Tot. Energy		Rel. Energy		n	Tot. Energy		Rel. Energy	
	DVR3D	TDQM	DVR3D	TDQM		DVR3D	TDQM	DVR3D	TDQM
1	1483.5	1483.6	0.0	0.0	1	1421.4	1421.4	0.0	0.0
2	2290.6	2289.9	807.0	806.3	2	2195.3	2195.3	773.9	773.9
3	2294.3	2295.6	810.8	811.9	3	2208.4	2208.5	787.1	787.1
4	2613.6	2613.4	1130.1	1129.8	4	2517.1	2517.2	1095.8	1095.8
5	3059.8	3059.8	1576.3	1576.2	5	2943.9	2944.0	1522.6	1522.6
6	3112.0	3112.1	1628.5	1628.4	6	3000.4	3000.5	1579.1	1579.1
7	3241.2	3241.2	1757.6	1757.5	7	3127.4	3127.5	1706.0	1706.1
8	3265.9	3265.9	1782.3	1782.3	8	3140.9	3141.0	1719.5	1719.6
9	3408.8	3408.7	1925.3	1925.1	9	3290.3	3290.4	1869.0	1869.0
10	3748.0	3748.2	2264.5	2264.6	10	3615.8	3615.9	2194.4	2194.5
11	3831.6	3831.6	2348.1	2348.0	11	3695.3	3695.3	2273.9	2273.9
12	3933.5	3933.6	2450.0	2449.9	12	3799.7	3799.7	2378.3	2378.3
13	4002.1	4002.2	2518.6	2518.6	13	3869.1	3869.2	2447.8	2447.8
14	4016.5	4016.5	2533.0	2532.9	14	3871.8	3872.0	2450.5	2450.6
15	4076.7	4076.6	2593.2	2593.0	15	3926.0	3926.1	2504.6	2504.7
16	4175.5	4176.2	2691.9	2692.5	16	4033.4	4033.5	2612.0	2612.1
17	4202.4	4202.4	2718.8	2718.7	17	4061.5	4061.5	2640.1	2640.2
18	4482.9	4483.0	2999.4	2999.4	18	4332.5	4332.6	2911.1	2911.2
19	4508.9	4509.0	3025.4	3025.3	19	4355.5	4355.6	2934.1	2934.2
20	4604.6	4604.7	3121.1	3121.1	20	4449.7	4449.8	3028.4	3028.4

A comparison between the bound state energies and assignments from the present and previ-

ous^{10,11} work is given in Table 2. A first investigation of the lower bound states was carried out on 3-dimensional PES (“near-equilibrium” PES¹⁰) based on internally contracted CI calculations and a basis set similar to a Dunning cc-VQZ basis set. This PES was fitted to a parametrized form and the bound states were determined variationally.¹⁰ In later work,¹¹ Born Oppenheimer dynamics were run at the B3PW91/6-31G(d,p) level of theory at 283 K and 700 K and spectroscopic features were extracted from the Fourier transform of the velocity autocorrelation function.

Table 2: Lower bound states (in cm^{-1}) from the literature^{10,11} and the present work. The assignment to harmonic quantum numbers ν_1 (symmetric stretch), ν_2 (bend), and ν_3 (antisymmetric stretch) by node-counting is approximate due to strong couplings between the modes. The vibrational angular momentum quantum number is l .

$\nu_1\nu_2\nu_3l$	Ref. ¹¹	Ref. ¹⁰	CCSD(T)-F12	MRCI+Q
0 1 0 1	393	426	406	395
0 0 1 0	900	929	807	774
0 2 0 0	785	851	811	787
1 0 0 0	1040	1190	1130	1096
0 1 1 1	1238	1334	1193	1150
0 3 0 1	1173	1281	1220	1184
1 1 0 1	1402	1614	1529	1484
0 2 1 0	1681	1739	1576	1523
0 4 0 0	1561	1709	1629	1579
0 0 2 0	1795	1883	1758	1706
1 0 1 0	1905	1943	1782	1720
1 2 0 0	1991	2038	1925	1869
0 3 1 1	2141	2148	1963	1899
0 5 0 1	2130	2141	2040	1979
0 1 2 1	2260	2281	2139	2078
1 1 1 1	2390	2344	2160	2088
2 0 0 0	2420	2396	2265	2194
1 3 0 1		2466	2324	2256

It is observed that for the (100) symmetric stretch level (see Table 2) the present CCSD(T) calculations are consistent with earlier calculations on a 3d-PES¹⁰ and with experiment but less so for the *ab initio* MD simulations.¹¹ Also, the MRCI+Q calculations find the ν_1 mode at 1096 cm^{-1} , 74 cm^{-1} below the experimental value (1170 cm^{-1}) and almost 100 cm^{-1}

below the value obtained from the earlier bound state calculations.¹⁰ All methods agree that the (001) antisymmetric stretch level lies below the (100) stretch which points towards an unusual shape of the PES. For the different methods used here this excitation is between 774 cm^{-1} and 807 cm^{-1} which compares with frequencies at 900 cm^{-1} or above from previous work.^{10,11} Finally, the (010) bending vibration level is predicted to lie at around 400 cm^{-1} by all calculations. For these two fundamentals no experimental data are available. The zero point energy from the present calculations is 1484 cm^{-1} on the CCSD(T)-F12/aug-cc-pVTZ-f12 PES and 1421 cm^{-1} on the MRCI PES, compared with 1524 cm^{-1} on the earlier 3d-PES.¹⁰

The higher vibrational states (combination bands and overtones) and their approximate assignments in terms of harmonic quantum numbers are listed in Table 2. Assignments of quantum numbers were made based on node counting but due to the strong couplings for certain states, the labels for the quantum numbers are rather approximate. As with the previous comparison between bound states on the previous 3d-PES¹⁰ and the BO-dynamics,¹¹ differences exist with the present calculations. This is already expected based on the observations for the fundamentals above, but also due to the anharmonic nature of many vibrations and the strong couplings between them. It is found that the bound states calculated on the MRCI+Q and CCSD(T)-F12 PESs from the present work are consistent but can differ by several 10 cm^{-1} . Thus, the MRCI calculations, albeit somewhat lower in accuracy than the CCSD(T)-F12 approach, provide a realistic description of the energetics and couplings. Also, typically, the bound states on these two PESs are lower than those on the previous PES,¹⁰ sometimes by up to 200 cm^{-1} . This may be due to both the overall shape of the PES and the nature of the anharmonic couplings. A few representative wavefunctions are reported in Figure 8.

Independently, the gas phase fundamentals for N_3^+ were also obtained from the power spectra

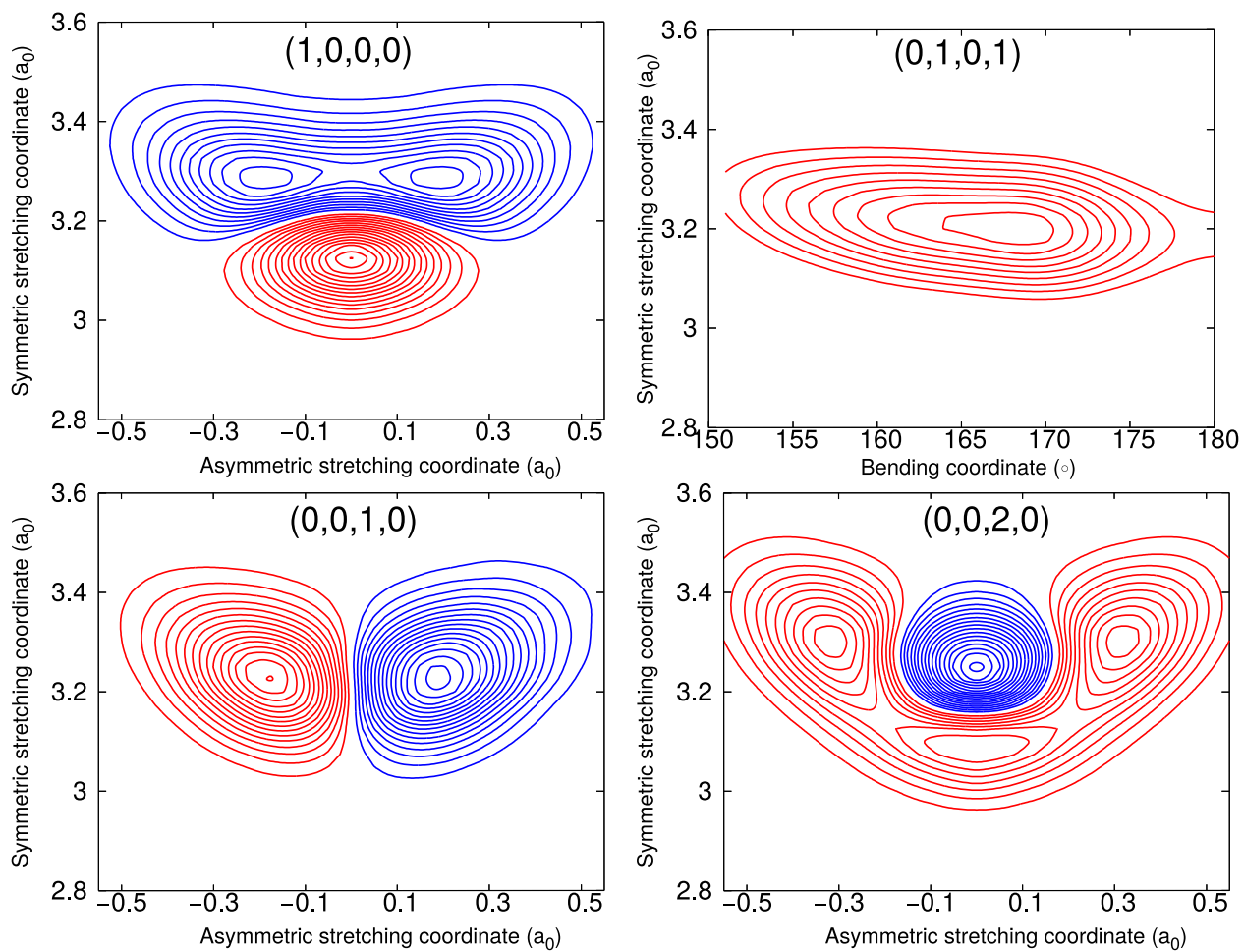


Figure 8: Wavefunctions from DVR3D calculations for several low energy states, as indicated by the labels $(\nu_1\nu_2\nu_3l)$.

of the N-N distances using MD simulations.³⁶ For this, *NVE* simulations were run using CHARMM³⁷ with the RKHS-interpolated CCSD(T)-F12b PES at a temperature of 10 K. The ν_1 , ν_2 , and ν_3 modes of N_3^+ are found to lie at 1275 cm^{-1} , 357 cm^{-1} and 917 cm^{-1} , respectively, consistent with the DVR3D results, see Table 2.

Conclusions

The current work focuses on the three dimensional PES and the low-lying vibrations of the N_3^+ radical cation in its $^3\Sigma_g^-$ ground state through electronic structure and rigorous quantum bound state calculations. Ab initio energies at the CCSD(T)-F12b and MRCI+Q level of theory were represented as a reproducing kernel Hilbert space (RKHS) to generate PESs for the electronic ground state of the ion. A detailed analysis of the electronic structure of the ground state PES was performed to assess the validity of Hartree-Fock as a reference wave function for coupled cluster and to rationalize the topology of the PESs. The multireference character of the electronic structure may vary from a) “absent” around the global minimum of the PES to b) “weak” along the dissociation paths with one covalent N-N bond only mildly stretched, and c) “strong” when two covalent bonds are stretched far from their equilibrium distance at the same time. For this latter case the role of energetically low lying charge transfer states was also investigated.

The vibrational bound states supported by each PES are calculated by solving the time-independent and time-dependent nuclear Schrödinger equation. For the symmetric stretching frequency, the only one available from experiment, quite good agreement is found with the results on the CCSD(T)-F12 PES. Further verification of the calculated vibrational frequencies is provided through calculations on an MRCI+Q PES and power spectra determined from MD simulations. In summary, it is found that single-reference open-shell coupled clus-

ter theory is able to yield a reliable high-quality PES for the vibrational bound states of the electronic ground state of N_3^+ .

This work demonstrates that MRCI+Q calculations provide a realistic description of the energetics of this challenging system by direct comparison with vibrational states from CCSD(T)-F12 calculations, both methods using an aug-cc-pVTZ basis set. As the higher electronically excited states require explicit inclusion of multi reference effects, the present work also lays the groundwork for future exploration of the reactive dynamics of the N_3^+ ion, similar to previous studies of other N-containing neutrals, such as $\text{C}+\text{NO}$ ³⁸ or $\text{N}+\text{NO}$.³⁹ For this, further studies of electronically excited states of N_3^+ are required.

Acknowledgment

Support by the Swiss National Science Foundation through grants 200021-117810, the NCCR MUST (to MM), and the University of Basel is also acknowledged. Part of this work was supported by the United State Department of the Air Force, which is gratefully acknowledged (to MM). This work was supported by the Australian Research Council Discovery Project Grants (DP150101427, DP160100474). The authors acknowledge fruitful discussions with Prof. Stefan Willitsch. MM acknowledges the Department of Chemistry of Melbourne University for a Wilsmore Fellowship during which this work has been initiated.

References

- (1) de Petris, G.; Cartoni, A.; Angelini, G.; Ursini, O.; Bottoni, A.; Calvaresi, M. The N_3^+ reactivity in ionized gases containing sulfur, nitrogen, and carbon oxides. *ChemPhysChem* **2006**, *7*, 2105–2114.

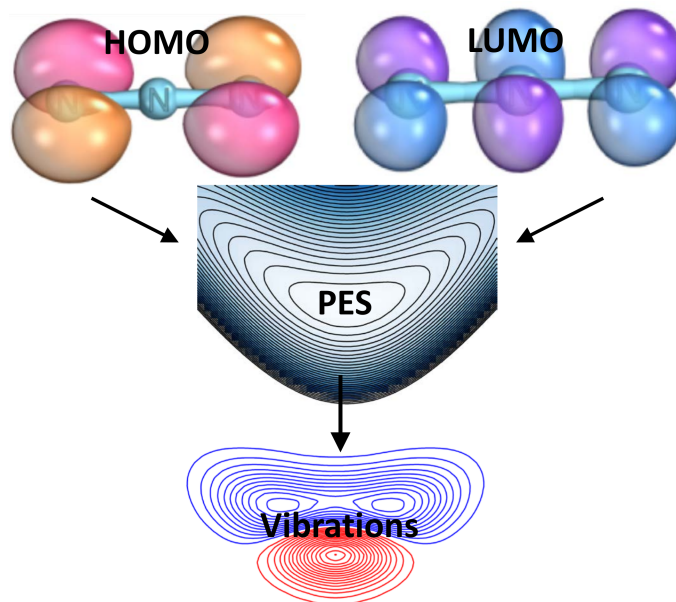


Figure 9: TOC graphics

- (2) Anicich, V.; Milligan, D.; Fairley, D.; McEwan, M. Thermomolecular ion-molecule reactions in Titan's atmosphere, I - Principal ions with principal neutrals. *Icarus* **2000**, *146*, 118–124.
- (3) Bennett, F. R.; Maier, J. P.; Chambaud, G.; Rosmus, P. Photodissociation, charge and atom transfer processes in electronically excited states of N_3^+ . *Chem. Phys.* **1996**, *209*, 275 – 280.
- (4) Midey, A.; Miller, T.; Viggiano, A. Reactions of N^+ , N_2^+ , and N_3^+ with NO from 300 to 1400 K. *J. Chem. Phys.* **2004**, *121*, 6822–6829.
- (5) Friedmann, A.; Soliva, A.; Nizkorodov, S.; Bieske, E.; Maier, J. $A^3\Pi_u - X^3\Sigma_g^-$ electronic spectrum of N_3^+ . *J. Phys. Chem.* **1994**, *98*, 8896–8902.
- (6) Dyke, J.; Jonathan, N.; Lewis, A.; Morris, A. Vacuum ultraviolet photoelectron spectroscopy of transient species. *Mol. Phys.* **1982**, *47*, 1231–1240.
- (7) Archibald, T. W.; Sabin, J. R. Theoretical investigation of the electronic structure and properties of N_3^- , N_3 , and N_3^+ . *J. Chem. Phys.* **1971**, *55*, 1821–1829.

- (8) Cai, Z.-L.; Wang, Y.-F.; Xiao, H.-M. Ab initio study of low-lying electronic states of the N_3^+ ion. *Chem. Phys.* **1992**, *164*, 377 – 381.
- (9) Tian, R.; Facelli, J.; Michl, J. Vibrational and electronic spectra of matrix-isolated N_3 and N_3^- . *J. Phys. Chem.* **1988**, *92*, 4073–4079.
- (10) Chambaud, G.; Rosmus, P.; Bennett, F.; Maier, J.; Spielfiedel, A. Vibrational motion in the $X^3\Sigma_g^-$ - state of N_3^+ . *Chem. Phys. Lett.* **1994**, *231*, 9–12.
- (11) Jolibois, F.; Maron, L.; Ramirez-Solis, A. Ab initio molecular dynamics studies on the lowest triplet and singlet potential surfaces of the azide cation: Anharmonic effects on the vibrational spectra of linear and cyclic N_3^+ . *J. Mol. Struct.-THEOCHEM* **2009**, *899*, 9–17.
- (12) Werner, H.-J.; Knowles, P. J.; Knizia, G.; Manby, F. R.; Schütz, M. Molpro: A general-purpose quantum chemistry program package. *WIREs Comput. Mol. Sci.* **2012**, *2*, 242–253.
- (13) Werner, H.-J.; Knowles, P. J.; Knizia, G.; Manby, F. R.; et al., M. S. MOLPRO, version 2019.1, A package of ab initio programs. 2019.
- (14) Knizia, G.; Adler, T. B.; Werner, H.-J. Simplified CCSD(T)-F12 methods: Theory and benchmarks. *J. Chem. Phys.* **2009**, *130*, 054104.
- (15) Peterson, K. A.; Adler, T. B.; Werner, H.-J. Systematically convergent basis sets for explicitly correlated wavefunctions: The atoms H, He, B-Ne and Al-Ar. *J. Chem. Phys.* **2008**, *128*, 084102.
- (16) Werner, H.-J.; Knowles, P. J. An efficient internally contracted multiconfiguration-reference configuration interaction method. *J. Chem. Phys.* **1988**, *89*, 5803–5814.

- (17) Knowles, P. J.; Werner, H.-J. An efficient method for the evaluation of coupling coefficients in configuration interaction calculations. *Chem. Phys. Lett.* **1988**, *145*, 514 – 522.
- (18) Dunning, T. H. Gaussian basis sets for use in correlated molecular calculations. I. The atoms boron through neon and hydrogen. *J. Chem. Phys.* **1989**, *90*, 1007–1023.
- (19) Langhoff, S.; Davidson, E. Configuration interaction calculations on nitrogen molecule. *Int. J. Quant. Chem.* **1974**, *8*, 61–72.
- (20) Werner, H.-J.; Knowles, P. J. A second order multiconfiguration SCF procedure with optimum convergence. *J. Chem. Phys.* **1985**, *82*, 5053–5063.
- (21) Knowles, P. J.; Werner, H.-J. An efficient second-order MC SCF method for long configuration expansions. *Chem. Phys. Lett.* **1985**, *115*, 259 – 267.
- (22) Werner, H.-J.; Meyer, W. A quadratically convergent multiconfiguration-selfconsistent field method with simultaneous optimization of orbitals and CI coefficients. *J. Chem. Phys.* **1980**, *73*, 2342–2356.
- (23) Kreplin, D. A.; Knowles, P. J.; Werner, H.-J. Second-order MCSCF optimization revisited. I. Improved algorithms for fast and robust second-order CASSCF convergence. *J. Chem. Phys.* **2019**, *150*.
- (24) Ho, T.-S.; Rabitz, H. A general method for constructing multidimensional molecular potential energy surfaces from ab initio calculations. *J. Chem. Phys.* **1996**, *104*, 2584–2597.
- (25) Unke, O. T.; Meuwly, M. Toolkit for the construction of Reproducing Kernel-Based representations of data: Application to multidimensional potential energy surfaces. *J. Chem. Inf. Model.* **2017**, *57*, 1923–1931.

- (26) Tennyson, J.; Kostin, M. A.; Barletta, P.; Harris, G. J.; Polyansky, O. L.; Ramanlal, J.; Zobov, N. F. DVR3D: a program suite for the calculation of rotation-vibration spectra of triatomic molecules. *Comput. Phys. Commun.* **2004**, *163*, 85 – 116.
- (27) Dai, J.; Zhang, J. Z. H. Time-dependent spectral calculation of bound and resonance energies of HO₂. *J. Chem. Phys.* **1996**, *104*, 3664–3671.
- (28) Koner, D.; Barrios, L.; González-Lezana, T.; Panda, A. N. Scattering study of the Ne + NeH⁺($v_0 = 0, j_0 = 0$) → NeH⁺ + Ne reaction on an ab initio based analytical potential energy surface. *J. Chem. Phys.* **2016**, *144*, 034303.
- (29) Koner, D. *Scattering studies of proton transfer reactions between rare gas atoms*; Indian Institute of Technology Guwahati, 2016.
- (30) Feit, M. D.; J. A. Fleck, J.; Steiger, A. Solution of the Schrödinger equation by a spectral method. *J. Comp. Phys.* **1982**, *47*, 412 – 433.
- (31) Dai, J.; Zhang, J. Z. H. Noise-free spectrum for time-dependent calculation of eigenenergies. *J. Chem. Phys.* **1995**, *103*, 1491–1497.
- (32) Mahapatra, S.; Sathyamurthy, N. Correlation function approach to transition state resonances in collinear (He,H₂⁺) collisions. *J. Chem. Phys.* **1995**, *102*, 6057–6066.
- (33) Iboview: Orbital visualization program, G. Knizia <https://www.iboview.org>, Accessed: 09.04.2020.
- (34) Trickl, T.; Cromwell, E. F.; Lee, Y. T.; Kung, A. H. State-selective ionization of nitrogen in the X²Σ_g⁺($v_+ = 0$) and ($v_+ = 1$) states by two-color (1+1) photon excitation near threshold. *J. Chem. Phys.* **1989**, *91*, 6006–6012.
- (35) Lide, D. R. *CRC Handbook of Chemistry and Physics*, 88th ed.; CRC Press, 2007.
- (36) Salehi, S. M.; Koner, D.; Meuwly, M. Vibrational Spectroscopy of N₃⁻ in the gas and condensed phase. *J. Phys. Chem. B* **2019**, *123*, 3282–3290.

- (37) Brooks, B. R. et al. CHARMM: The biomolecular simulation program. *J. Comput. Chem.* **2009**, *30*, 1545–1614.
- (38) Koner, D.; Bemish, R. J.; Meuwly, M. The $C(^3P) + NO(X^2\Pi) \rightarrow O(^3P) + CN(X^2\Sigma^+)$, $N(^2D)/N(^4S) + CO(X^1\Sigma^+)$ reaction: Rates, branching ratios, and final states from 15 K to 20 000 K. *J. Chem. Phys.* **2018**, *149*, 094305.
- (39) San Vicente Veliz, J. C.; Koner, D.; Schwilk, M.; Bemish, R. J.; Meuwly, M. The $N(^4S) + O_2(X^3\Sigma_g^-) \leftrightarrow O(^3P) + NO(X^2\Pi)$ reaction: thermal and vibrational relaxation rates for the $^2A'$, $^4A'$ and $^2A''$ states. *Phys Chem Chem Phys.* **2020**, *22*, 3927–3939.

Supporting Information: N_3^+ : Full-Dimensional Potential Energy Surface, Vibrational Fundamental and Dynamics on the Ground State

Debasish Koner,[†] Max Schwilk,[†] Sarbani Patra,[†] Evan J. Bieske,[‡] and Markus
Meuwly*,[¶]

[†]*Department of Chemistry, University of Basel, Klingelbergstrasse 80, CH-4056 Basel,
Switzerland*

[‡]*Department of Chemistry, University of Melbourne, Parkville 3010, Australia*

[¶]*Department of Chemistry, University of Basel,
Klingelbergstrasse 80, 4056 Basel, Switzerland*

E-mail: m.meuwly@unibas.ch

April 28, 2020

Table S1: Grid details for the triatomic N_3^+ potentials. Units are a.u.

	CCSD(T)-F12b	MRCI+Q
N_R	30	29
R_{\min}	1.7	2.2
R_{\max}	10.0	10.0
N_r	18	22
r_{\min}	1.5	1.55
r_{\max}	3.1	4.0
N_θ	13	7

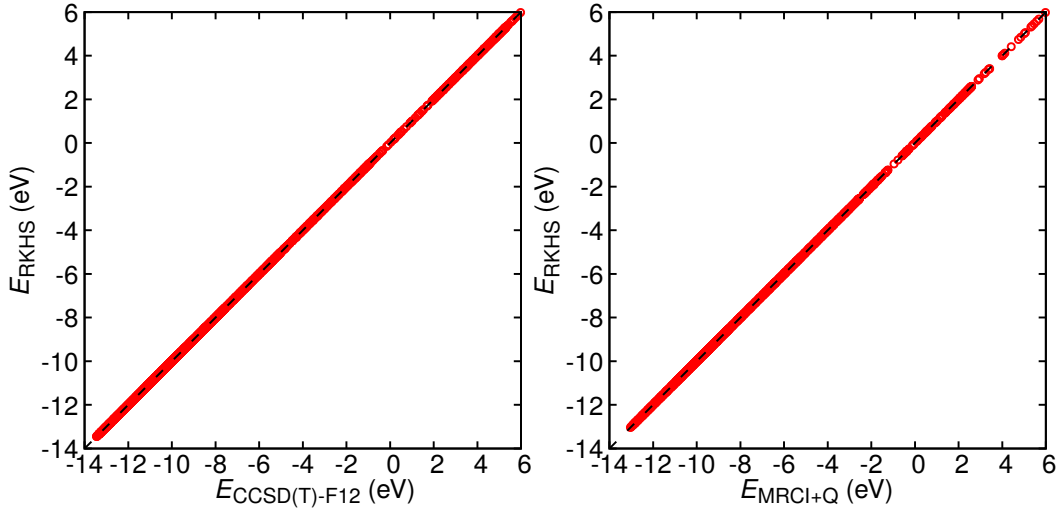


Figure S1: Correlation between *ab initio* and RKHS energies for the on-grid points. The zero of energy is the $E_N + E_N + E_{N+}$ asymptote. Left panel for the CCSD(T)-F12b PES and right panel for the MRCI+Q PES. The respective correlation coefficients are $R_{\text{CCSD(T)}}^2 = 1 - 4 \times 10^{-7}$ and $R_{\text{MRCI}}^2 = 1 - 3 \times 10^{-7}$.

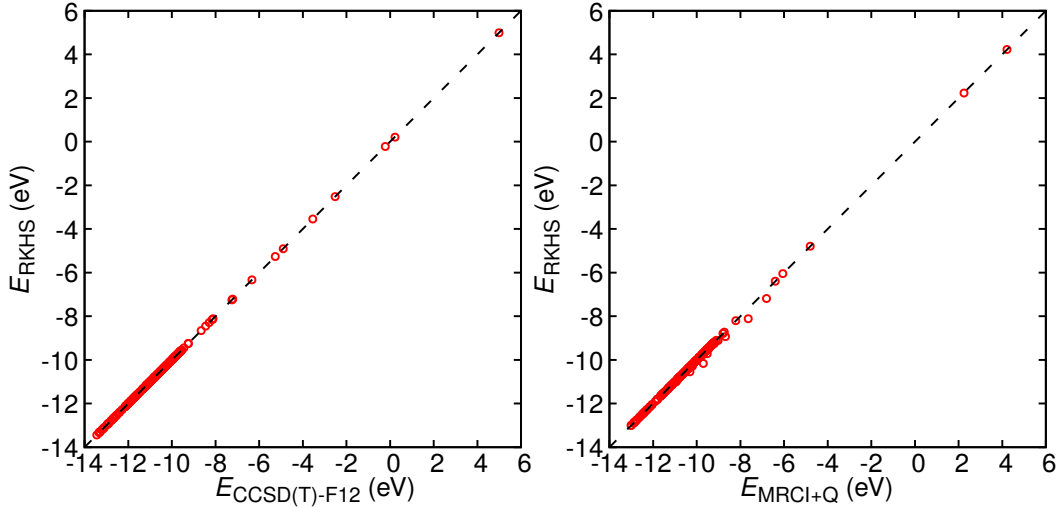


Figure S2: Correlation between *ab initio* and RKHS-interpolated energies for off-grid points at the CCSD(T)-F12b (left) and MRCI+Q (right) levels of theory. The zero of energy is the $E_N + E_N + E_{N+}$ asymptote. The respective correlation coefficients are $R_{\text{CCSD(T)}}^2 = 0.9999$ and $R_{\text{MRCI}}^2 = 0.9993$.

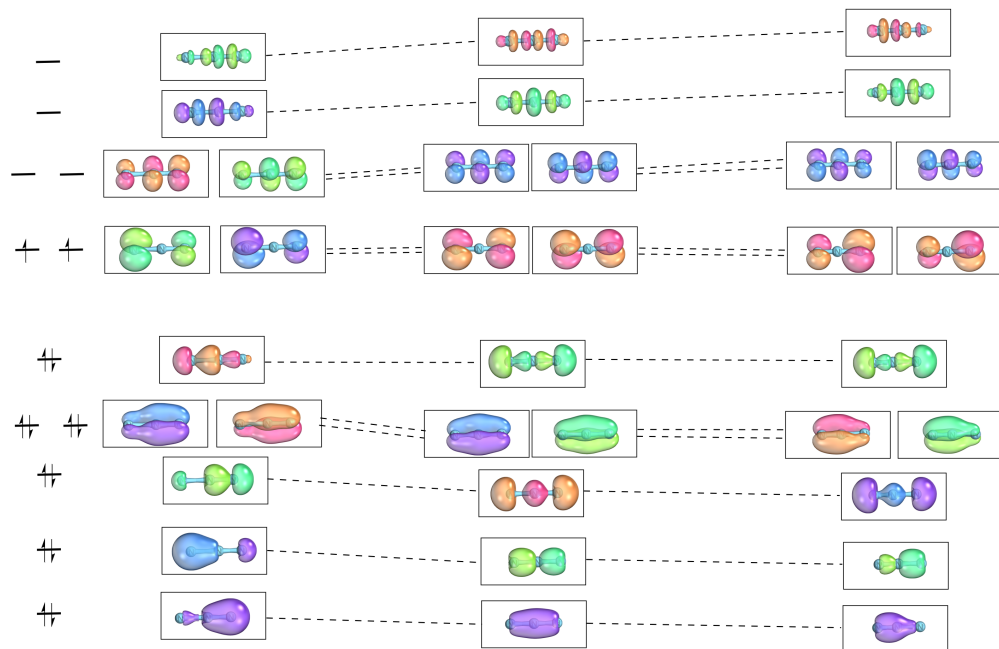


Figure S3: MO diagram of the evolution of the valence space natural orbitals for the triplet state linear bonding of N^+ to N_2 : Formation of covalent bonds (left panel), equilibrium structure (middle), and very small value of R .

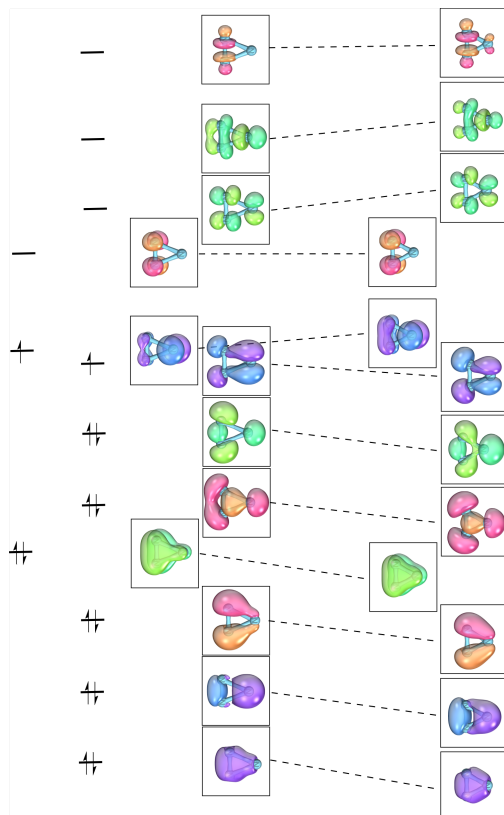


Figure S4: MO diagram of the evolution of the valence space natural orbitals for the T-shaped bonding of N^+ to N_2 : Formation of covalent bonds (left panel) and triangular structure with three nearly equidistant bonds.

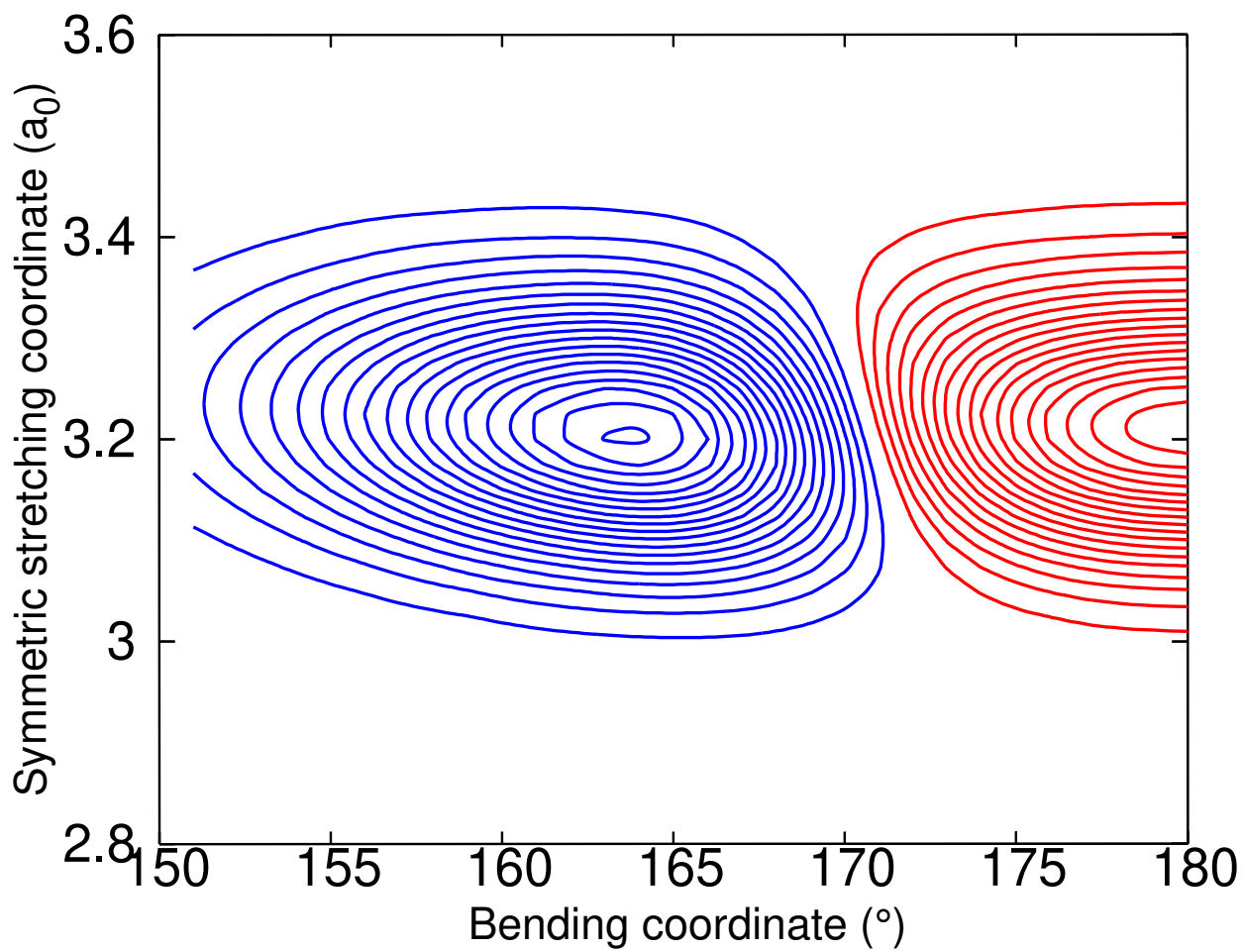


Figure S5: Wavefunction for the (0 2 0 0) state.

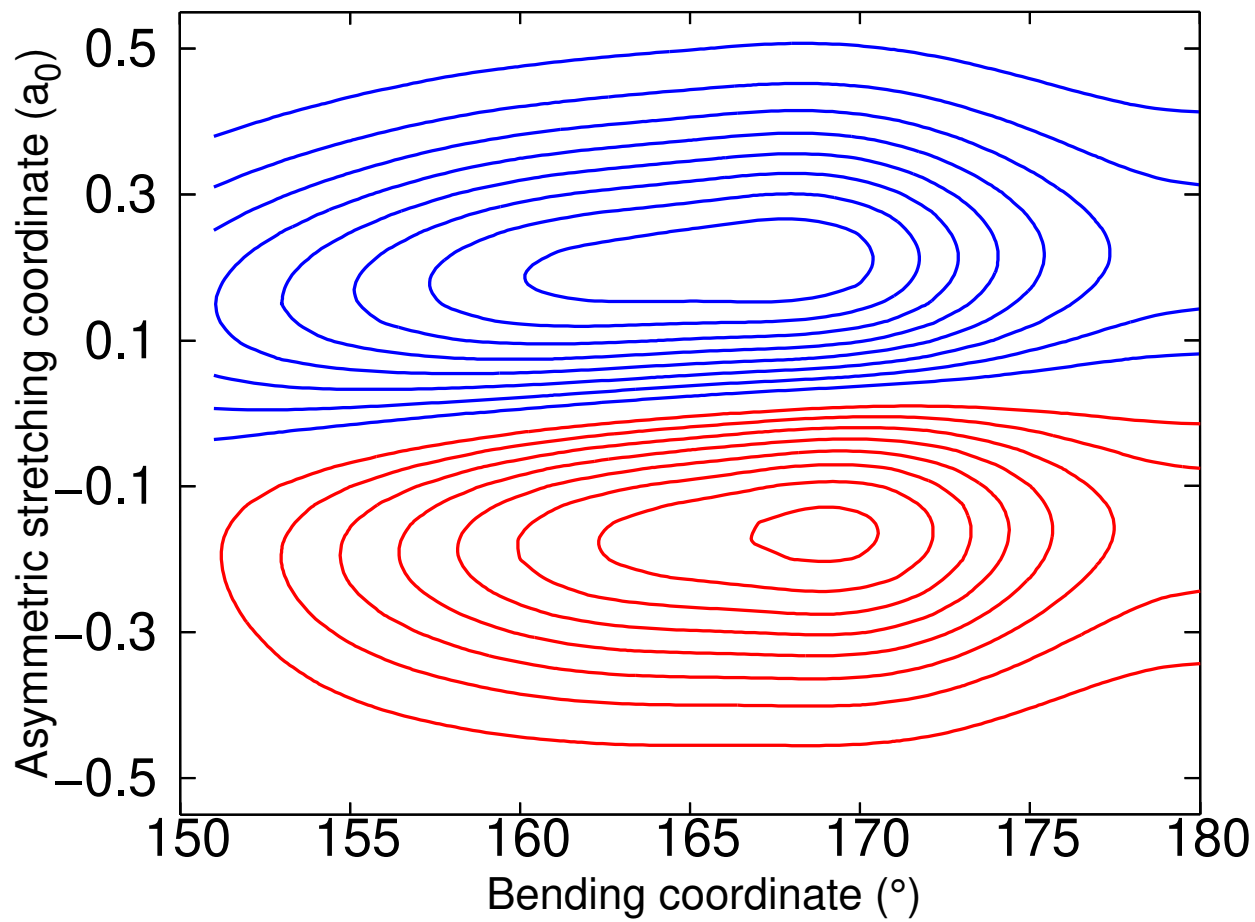


Figure S6: Wavefunction for the (0 1 1 1) state.

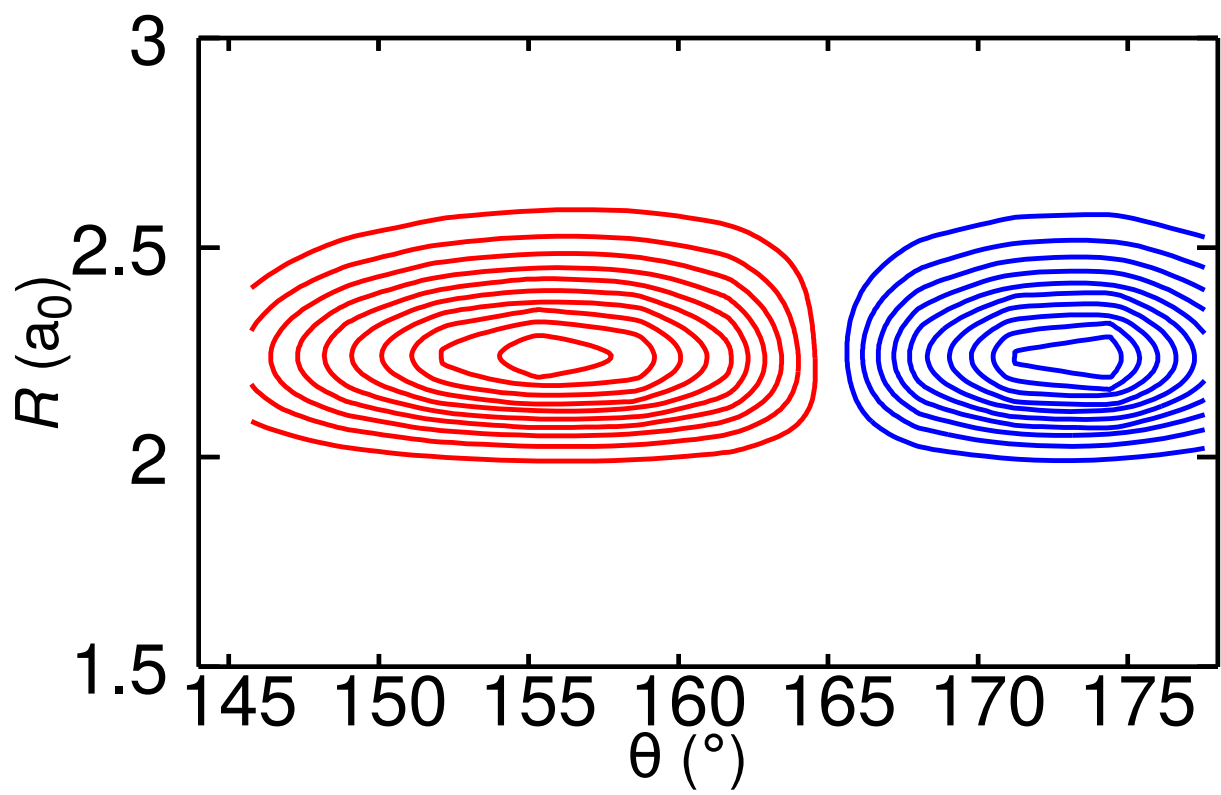


Figure S7: Wavefunction for the $(0\ 3\ 0\ 1)$ state.

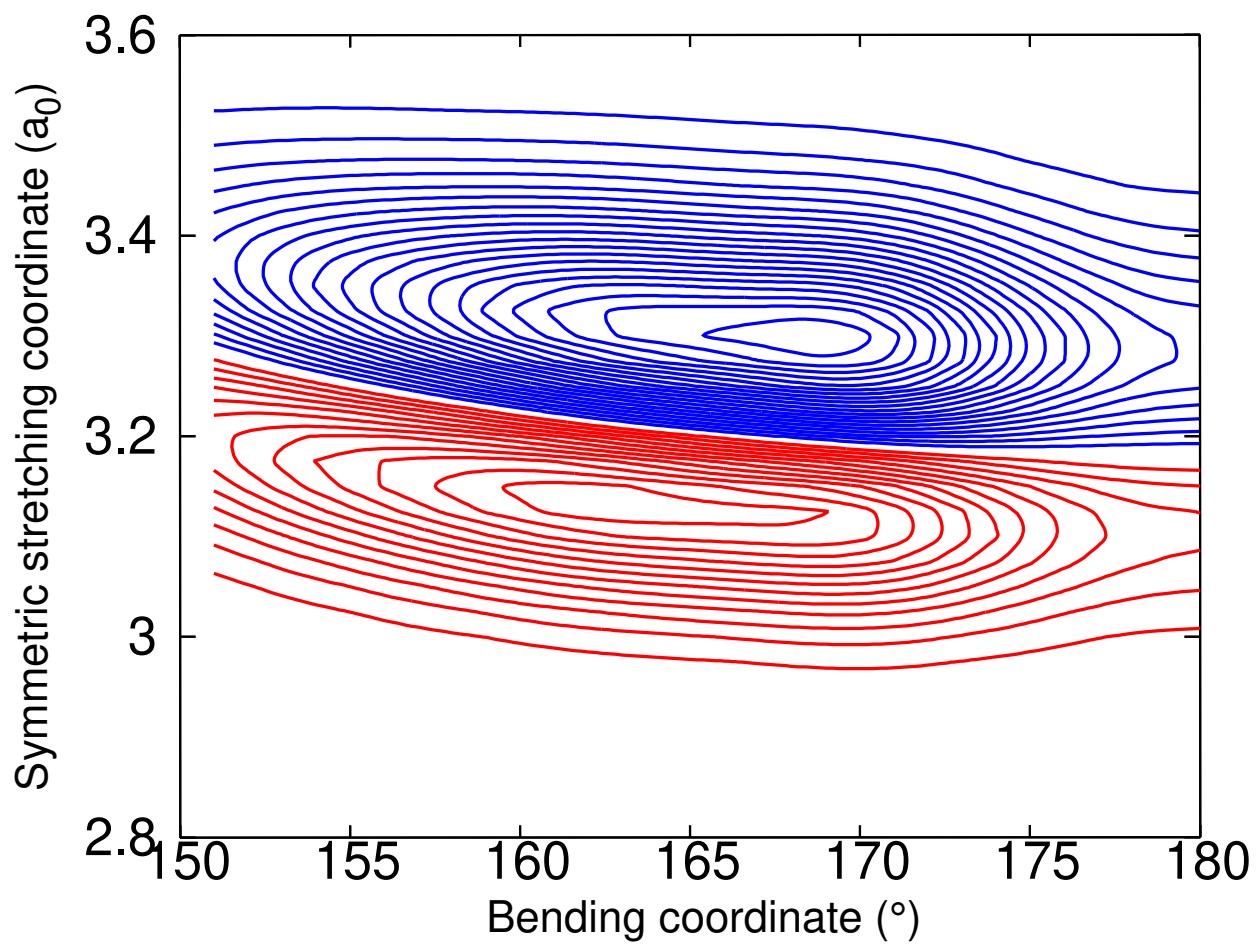


Figure S8: Wavefunction for the $(1\ 1\ 0\ 1)$ state.

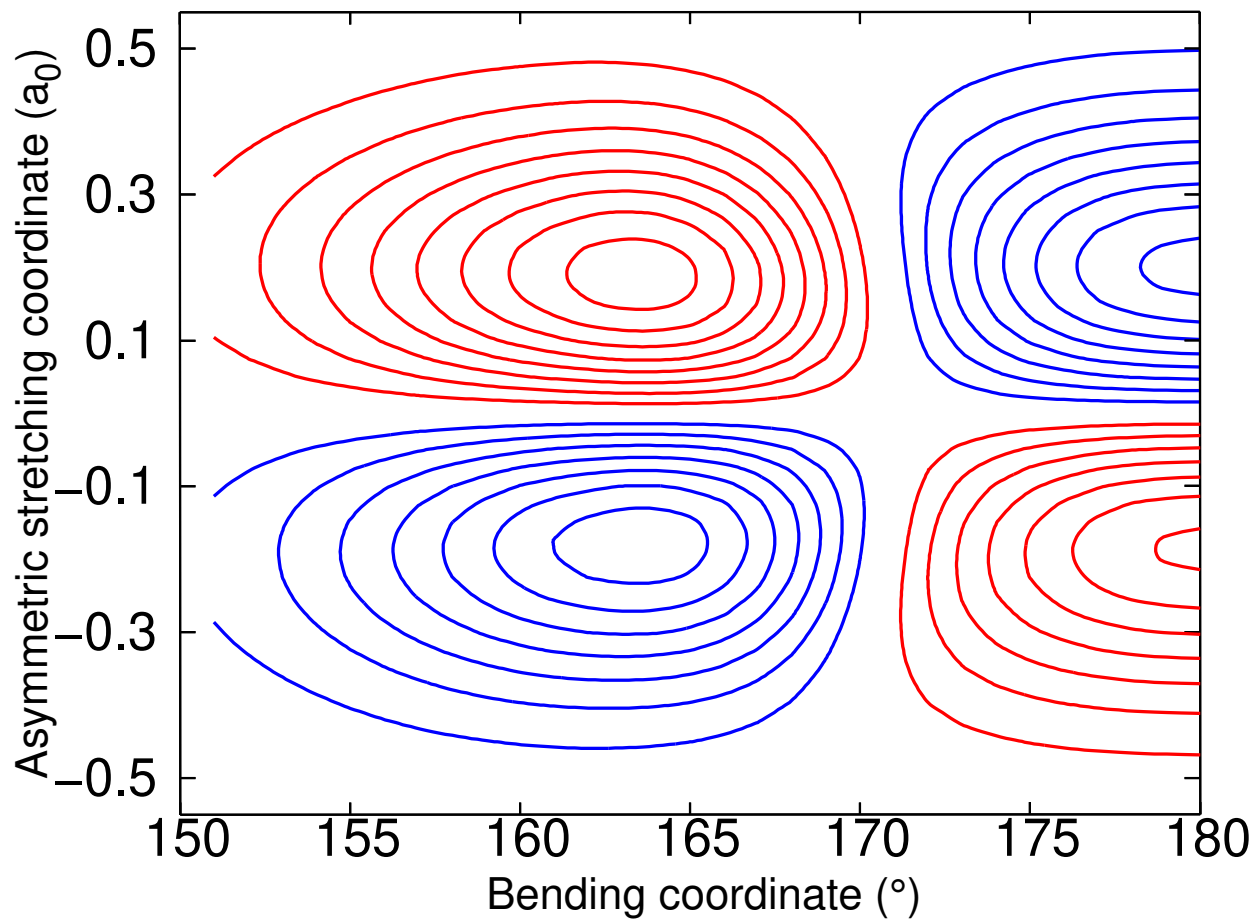


Figure S9: Wavefunction for the $(0\ 2\ 1\ 0)$ state.

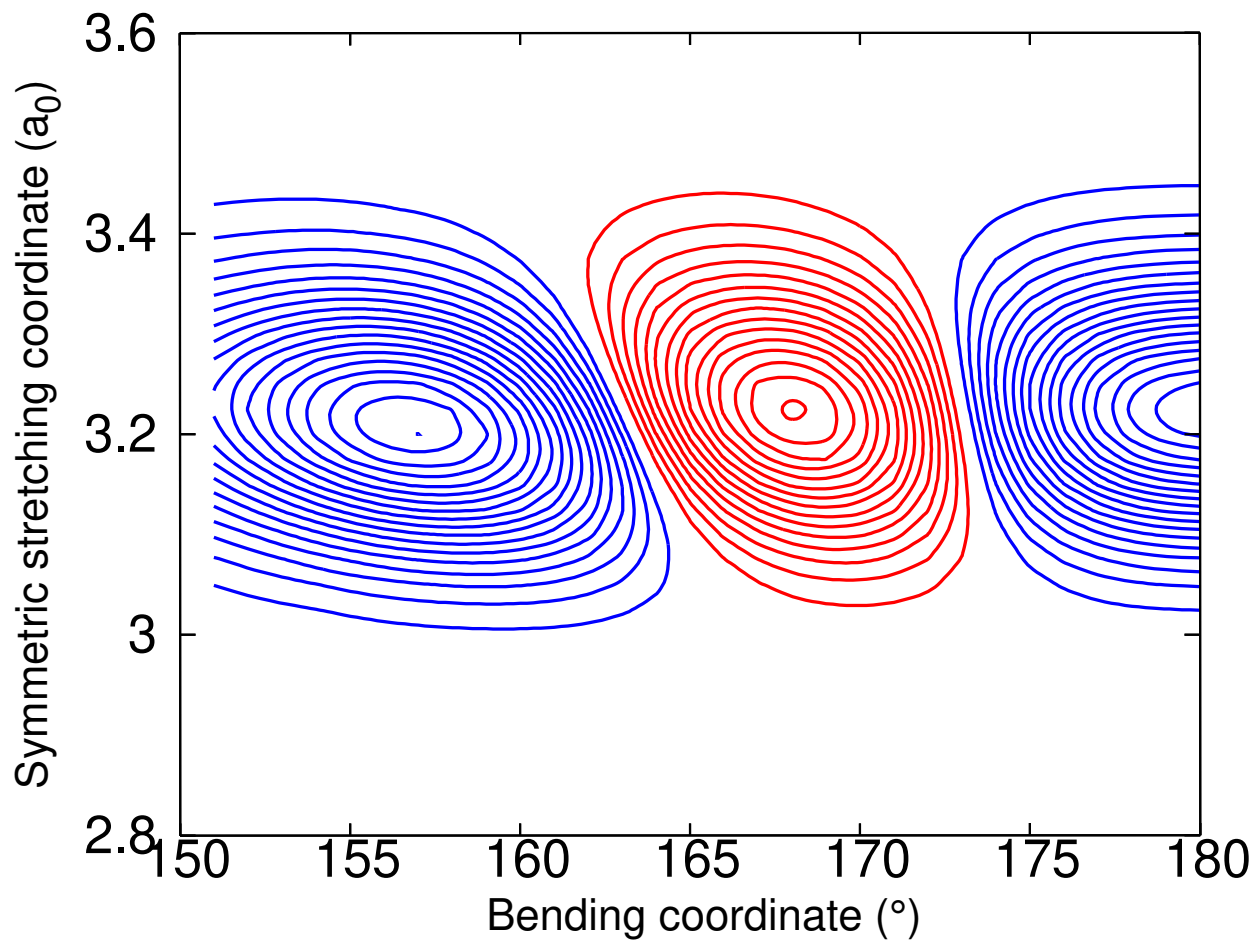


Figure S10: Wavefunction for the (0 4 0 0) state.